STRUCTURED H∞ DESIGN OF PREDICTORS FOR THE MONITORING OF AN AIRCRAFT IN ITS FLIGHT ENVELOPE

Karl Heinz Kienitz[1], Antonio González Sorribes[2], Ricardo Sanz Díaz[2], Celso Braga de Mendonça[3] & Pedro José García[2]

[1]Instituto Tecnológico de Aeronáutica, São José dos Campos, Brazil
[2]Instituto de Automática e Informática Industrial, Universitat Politècnica de València, Spain
[3]Boeing Brasil, São José dos Campos, Brazil

Abstract

Observers are proposed for predictive flight envelope monitoring. Gain design options are introduced and evaluated for a high-order observer-predictor structure. The aircraft is considered in longitudinal motion only. Modeling resorts to the nonlinear force equilibrium and kinematic equations. The prediction task is decomposed into a two-step process: (a) running observers provide predictions for longitudinal and vertical accelerations, pitch angle, and pitch rate; and (b) with these variable prediction histories available, the nonlinear model equation – then reduced to a linear time-varying equation – provides full state prediction through integration, thus enabling predictive monitoring of the aircraft in its flight envelope.

Keywords: prediction, disturbance observers, flight envelope, monitoring.

1. Introduction

Among the several relevant concepts in aircraft operation, one of the most critical is that of flight envelope. Flight envelopes are defined in a space of appropriately chosen variables, in which limits are set that guarantee safe flight. Other criteria may also be involved, e.g. efficiency. Suitable variables can be airspeed, loads, and altitude [1]. So-called flight envelope protection, which aims at keeping the system operating within the desirable regions that make up the flight envelope, has been well investigated and used ([2]-[4]), and improved methods for flight envelope prediction, in the sense of its adequate determination, have received attention in recent research endeavors (e.g. [5]-[6]).

To even better protect the aeronautical system during operations, this work is concerned with forecasting variables that enable predicting an aircraft's position within its flight envelope at time instants of interest. With suitable mathematical models and the relevant variables available, observer-predictors are constructs that are used herein to implement such prediction. Predicting the evolution of an aircraft in its flight envelope will entail relevant gains because safety margins might be optimized and operational warnings and precautionary system rescheduling improved and anticipated.

The contributions of this article are: (a) the discussion of prediction for flight envelope monitoring; and (b) the proposal of a solution to the prediction problem in flight scenarios with longitudinal motion. The proposed prediction scheme resorts to the force equilibrium and kinematic equations of aircraft motion, avoiding the use of detailed dynamic aircraft models. To solve the prediction task, a high-order observer-predictor structure proposed in [7] is considered. Its original LMI-based gain design is compared to other design options based on structured H∞ control design.

This paper is structured as follows. In Section 2 the model for aircraft motion and the prediction intended for flight envelope monitoring are presented. Section 3 is dedicated to observer-predictors and specific aspects of their use in the flight envelope monitoring endeavor. The critical observer gain design problem is dealt with in Section 4. Section 5 details practical considerations, and presents simulation results for an illustrative application of the concepts proposed in the paper. Conclusions are found in the final section.

2. Prediction Within a Flight Envelope

Following mainstream definitions and conventions (e.g. see [8]) the following variables are used in this text:

- p, q, and r are the projections of the angular rate vector of the aircraft along its body axes;
- u, v, and w are inertial speed projections along the aircraft body axes;
- θ is the pitch angle;
- φ is the roll angle;
- ψ is the yaw angle;
- a_x, a_y, and a_z are specific forces measured by typical accelerometers on the aircraft body axes.

For the purposes of this paper, an aircraft's flight envelope is a compact region in the plane defined by the variables total velocity (V) and load factor (n_z), given by

$$V = \sqrt{(u+u_w)^2 + (v+v_w)^2 + (w+w_w)^2}, n_z = \frac{\dot{w}}{g}, \tag{1}$$

Where g is the gravitational acceleration, and u_w, v_w, and w_w are wind vector components; these, however, will not be considered, i.e. $u_w = v_w = w_w = 0$.

The mathematical model of the aircraft in flight is given by the equations that describe the force equilibrium of aircraft motion along the body axes, and the equations that describe the kinematic of aircraft attitude related to the Earth's surface. These equations are widely used, for instance in flight path reconstruction problems, and here were taken from [9].

The equations resulting from force equilibrium considerations are:

$$\begin{aligned} \dot{u} &= rv - qw - g\sin(\theta) + a_x, \\ \dot{v} &= pw - ru + g\cos(\theta)\sin(\varphi) + a_y, \\ \dot{w} &= qu - pv + g\cos(\theta)\cos(\varphi) + a_z. \end{aligned} \tag{2}$$

The kinematic equations for aircraft attitude are:

$$\begin{aligned} \dot{\varphi} &= p + q\sin(\varphi)\tan(\theta) + r\cos(\varphi)\tan(\theta), \\ \dot{\theta} &= q\cos(\varphi) - r\sin(\varphi), \\ \dot{\psi} &= q\sin(\varphi)\sec(\theta) + r\cos(\varphi)\sec(\theta). \end{aligned} \tag{3}$$

The model defined by equations (2) and (3) is not affected by relevant uncertainties. Available measurements and calculated values, however, may be affected by noise.

As a simplified but realistic scenario, only the longitudinal equations are considered herein, which means that, by hypothesis, the aircraft has no relevant roll and yaw motions. The equations derived from (2) and (3) for this scenario are the first three of the set in (4); the fourth equation states that the angular rate q results from a specific moment m.

$$\begin{aligned} \dot{u} &= -qw - g\sin(\theta) + a_x, \\ \dot{w} &= qu + g\cos(\theta) + a_z, \\ \dot{\theta} &= q, \\ \dot{q} &= m. \end{aligned} \tag{4}$$

m, a_x, and a_z are exogenous variables, and it is assumed that the values of $u(t)$, $w(t)$, $\theta(t)$, $q(t)$, $a_x(t)$, and $a_z(t)$ are available at current time t.

The predictive flight envelope monitoring effort will consist of the use of observer-predictors, presented in

the sequel, to predict values of n_z and V in future time instants, using the available model and variable values (past and present).

The unavailability of future values of the exogenous variables is the main challenge for any prediction effort. Simply neglecting these values typically results in significant errors in the computed predictions. Better approaches use approximants, such as those in [7], [10], and their references. In [7] it is shown that if the driving signals are continuously differentiable at least one time, then useful approximations can be obtained via conventional high-order linear time invariant observers. Such approximations are implemented in [7] via state-predictors yielding better accuracy than earlier solutions in [10] and [11].

3. Observer Predictors

Observer-predictors considered herein have the structure proposed in [7] and apply to situations with underlying dynamics described by:

$$\begin{aligned} \dot{x}(t) &= Ax(t) + B_\omega \omega(t), \\ y(t) &= C_x x(t) + D_\omega \omega(t), \end{aligned} \tag{5}$$

where $x \in \mathbb{R}^n$ is a state vector, $y \in \mathbb{R}^p$ is an output vector, and $\omega \in \mathbb{R}^q$ is a disturbance vector differentiable at least r times. This is not the structure found in (4) because of the nonlinear terms in its first two expressions. It is, however, applied here to a system described by (4) to create separate (parallel running) observers for the prediction of a_x, a_z, and $[\theta, q]$ using the double integrator structure (for θ and q), seen in last two expressions in (4). Such predictions can then be propagated through the integration of the linear time-varying (LTV) system in (6) to get predicted u, w, and $\dot{w}$ histories. From such histories flight envelope information is then determined straightforwardly.

$$\begin{bmatrix} \dot{u} \\ \dot{w} \end{bmatrix} = \begin{bmatrix} 0 & -q \\ q & 0 \end{bmatrix} \begin{bmatrix} u \\ w \end{bmatrix} + \begin{bmatrix} -g\sin(\theta) + a_x \\ g\cos(\theta) + a_z \end{bmatrix} \tag{6}$$

For the prediction of $[\theta, q]$ histories, the observer-predictor structure adopted herein observes the extended state vector

$$\eta^T(t) = \begin{bmatrix} x^T(t) & \omega^T(t) & \dot{\omega}^T(t) & \cdots & \omega^{(r)T}(t) \end{bmatrix}^T \tag{7a}$$

$$\dot{\eta}(t) = \bar{A}\eta(t) + \bar{B}_\omega \omega^{(r+1)}(t) \tag{7b}$$

$$y(t) = \bar{C}\eta(t) \tag{7c}$$

$$\xi(t) = K(T)\eta(t) \tag{7d}$$

where

$$\bar{A} = \begin{bmatrix} A & B_\omega \Pi \\ 0 & \Psi \end{bmatrix}, \Psi = \begin{bmatrix} 0_{rq\times q} & I_{rq} \\ 0_{q\times q} & 0_{q\times rq} \end{bmatrix}, \Pi = \begin{bmatrix} I_q & 0_{q\times rq} \end{bmatrix},$$

$$\bar{C} = \begin{bmatrix} C_x & D_\omega & 0_{p\times rq} \end{bmatrix}, \bar{B}_\omega = \begin{bmatrix} 0_{(n+rq)\times q} \\ I_q \end{bmatrix},$$

and $K(T)$ is chosen such that $\xi(t)$ approximates $x(t+T)$ via a truncated Taylor-series using $x(t), \omega(t), \dot{\omega}(t), \ldots,$ and $\omega^{(r)}(t)$, all of them present in the extended state vector η. The expression for $K(T)$ is given in [7] as

$$K(T) = \begin{bmatrix} e^{AT} & \frac{T}{1!}\Gamma_{\omega,0}(T)B_\omega & \cdots & \frac{T^{(r+1)}}{(r+1)!}\Gamma_{\omega,r}(T)B_\omega \end{bmatrix} \tag{8}$$

with

$$\Gamma_{\omega,i}(T) = \sum_{j=0}^{\infty} \frac{(i+1)!}{(i+j+1)!} A^j T^j .$$

Thus

$$x(t+T) = \xi(t) + \mathrm{O}_r(t),$$

where $\mathrm{O}_r(t)$ is a bounded error term that depends on the prediction horizon T and the bound assumed

for $\omega^{(r+1)}$, the "next higher" derivative not included in the extended state vector η.

A Luenberger-type observer is then proposed as follows:

$$\dot{\hat{\eta}}(t) = (\bar{A} - L\bar{C})\hat{\eta}(t) + Ly(t),$$
$$\hat{\xi}(t) = K(T)\hat{\eta}(t),$$
$$\hat{x}(t+T) = \hat{\xi}(t),$$

resulting in observation errors given by

$$e_\eta = \eta - \hat{\eta},$$
$$\dot{e}_\eta = (\bar{A} - L\bar{C})e_\eta + \bar{B}_\omega \omega^{(r+1)}, \text{ and}$$
$$e_\xi = \xi - \hat{\xi} = K(T)(\eta - \hat{\eta}) = K(T)e_\eta.$$

L shall be chosen to guarantee observer stability and attain desired performance. Options for adequate choices are discussed in the next section.

When predicting a_x and a_z, however, there is no underlying system dynamics. Nevertheless an extended state vector similar to that in (7a) can be used, but without x components in it. In such a setting actually $x(t) = \omega(t)$, and the value of x at $(t+T)$ in terms of a Taylor expansion at time t is:

$$x(t+T) = \omega(t) + \frac{T}{1!}\dot{\omega}(t) + \cdots + \frac{T^{r+1}}{(r+1)!}\omega^{(r+1)}(\zeta), \zeta(\mathrm{t}) \in [t, t+T].$$

Thus, with derivatives up to $\omega^{(r)}$ included in η, a prediction neglecting higher-order terms can be formulated as

$$\hat{x}(t+T) = K(T)\eta(t), K(T) = \begin{bmatrix} 1 & \frac{T}{1!} & \frac{T^2}{2!} & \cdots & \frac{T^r}{r!} \end{bmatrix},$$

and matrices used in (7) "collapse" to

$$\bar{A} = \Psi = \begin{bmatrix} 0_{rq\times q} & I_{rq} \\ 0_{q\times q} & 0_{q\times rq} \end{bmatrix}, \bar{C} = \begin{bmatrix} I_q & 0_{p\times rq} \end{bmatrix}, \bar{B}_\omega = \begin{bmatrix} 0_{rq\times q} \\ I_q \end{bmatrix}.$$

For a_x and a_z prediction, tracking differentiators could also be used, such as the one proposed in [10].

4. Observer Gain Calculation

4.1 Method 1

This method stems from [7], where L is chosen by picking a solution P to the following system of Linear Matrix Inequalities (LMIs):

$$\begin{bmatrix} \bar{A}^T P + P\bar{A} - Y\bar{C} - \bar{C}^T Y + 2\delta P & P\bar{B}_\omega \\ \bar{B}_\omega^T P & -I_q \end{bmatrix} \le 0,$$
$$P - \alpha K^T(T)K(T) \ge 0,$$
$$N \otimes P + M \otimes (P\bar{A} - Y\bar{C}) + M^T \otimes (P\bar{A} - Y\bar{C})^T < 0,$$

and choosing $L = P^{-1}Y$. This guarantees e_η decay with a rate of δ to a ball with radius $\varepsilon_r(2\alpha\delta)^{-1/2}$, where ε_r is a bound on the first derivative of the disturbance not available in the expanded state vector, i.e. $||\omega^{(r+1)}(t)|| \le \varepsilon_r$. Furthermore, due to the third LMI above, the eigenvalues of $(\bar{A} - L\bar{C})$ belong to $\{z \in \mathbb{C} \mid N + zM + z^*M^T < 0\}$ with real matrices M and $N=N^T$. See [12] for details on such eigenvalue location enforcement.

4.2 Method 2

An alternative calculation of L can be envisioned based on an $H\infty$ approach derived from the Kalman-Yakubovich-Popov (KYP) lemma by observing that a sensible signal-based design goal for the observer-predictor is to ensure that the impact (evaluated with the $H\infty$ norm of the transfer matrix) from $\omega^{(r+1)}$ on e_ξ is made small. The KYP lemma states that, if $G(s) = \tilde{C}(sI - \tilde{A})^{-1}\tilde{B} + \tilde{D}$ is the transfer

matrix from u to y of the minimal state description

$$\dot{x} = \tilde{A}x + \tilde{B}u,$$
$$y = \tilde{C}x + \tilde{D}u,$$

then the following are equivalent:

- $\tilde{A}$ is Hurwitz and $||G(s)||_\infty < \gamma$;
- $\exists P > 0$ such that

$$\begin{bmatrix} \tilde{A}^T P + P\tilde{A} + \tilde{C}^T\tilde{C} & \tilde{C}^T\tilde{D} + P\tilde{B} \\ \tilde{D}^T\tilde{C} + \tilde{B}^T P & \tilde{D}^T\tilde{D} - \gamma^2 I \end{bmatrix} < 0.$$

Now one may associate $x \leftarrow e_\eta$, $u \leftarrow \omega^{(r+1)}$, $y \leftarrow e_\xi$. Then $\tilde{A} \leftarrow (\bar{A} - L\bar{C})$, $\tilde{B} \leftarrow \bar{B}_\omega$, $\tilde{C} \leftarrow K(T)$, $\tilde{D} \leftarrow 0$, and a predictor can be obtained by designing P and Y for small γ such that

$$\begin{bmatrix} \bar{A}^T P + P\bar{A} - Y\bar{C} - \bar{C}^T Y + K^T(T)K(T) & P\bar{B}_\omega \\ \bar{B}_\omega{}^T P & -\gamma^2 I \end{bmatrix} < 0, P > 0.$$

$L = P^{-1}Y$ will yield a predictor that guarantees an $H\infty$ norm of the transfer matrix from $\omega^{(r+1)}$ to e_ξ smaller than γ.

The approach above can be improved by adding frequency-dependent weights on the disturbance ω and the (possible) additive noise n, i.e. when the second equation in (5) is more realistically $y(t) = C_x x(t) + D_\omega \omega(t) + n(t)$. In such case, a design solution is sought with structured $H\infty$ synthesis [13] maintaining the design constraint $u = Lv$; thus the states to be fed back remain the same.

The extended plant, i.e. the plant with added weights, to be considered in structured $H\infty$ synthesis then is the one in Fig. 1. Structured $H\infty$ synthesis will yield $u = Lv$ such that the $H\infty$ norm of the transfer matrix from $[\omega^{(r+1)} \;\; n]^T$ to e_ξ is small under the given structural feedback constraint (i.e., $u = Lv$). Typical weight choices in $H\infty$ approaches are W_1 and W_2 diagonal matrices of first-order low-pass transfer functions and of first-order high-pass transfer functions respectively [14].

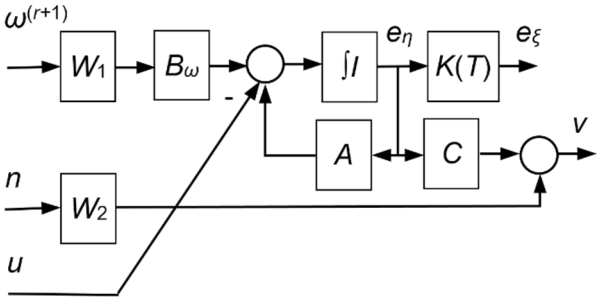

Figure 1 – Generalized plant for gain design with Method 2

4.3 Method 3

The underlying idea for a further gain design option can be derived from Method 2, also taking into consideration noise, but focusing on the error in the predicted value $x(t+T)$ rather than on $e_\xi(t)$, the driver in Method 2.

Considering the noise $n(t)$, the linear dynamics, instead of (5), are now given by

$$\dot{x}(t) = Ax(t) + B_\omega \omega(t),$$
$$y(t) = C_x x(t) + D_\omega \omega(t) + n(t).$$

Adopting a similar observer structure as in Methods 1 and 2, one uses the extended state vector η defined in (7). Thus

$$\dot{\eta}(t) = \bar{A}\eta(t) + \bar{B}[\omega^{(r+1)}(t) \quad n(t)]^T,$$
$$y(t) = \bar{C}\eta(t) + \bar{H}[\omega^{(r+1)}(t) \quad n(t)]^T,$$

with $\bar{A}$ as before, $\bar{C} = [C_x \;\; D_\omega \;\; 0 \;\; 0]$, $\bar{H} = [0 \;\; I]$, and

$$\bar{B}^T = \begin{bmatrix} 0 & 0 & \cdots & I \\ 0 & 0 & \cdots & 0 \end{bmatrix}^T.$$

The prediction at time t of the value of x at $(t+T)$ can be written as a Taylor expansion. For instance, writing up to the term of order 3 one has:

$$x(t+T) = \mathrm{e}^{AT}\, x(t) + \frac{T}{1!}\Gamma_{\omega,0}(T)B_\omega\omega(t) + \frac{T^2}{2!}\Gamma_{\omega,1}(T)B_\omega\dot{\omega}(t) +$$
$$+\frac{T^3}{3!}\Gamma_{\omega,2}(T)B_\omega\ddot{\omega}(t) + \frac{T^4}{4!}\Gamma_{\omega,3}(T)B_\omega\ddot{\omega}(\zeta(\mathrm{t})), \zeta(\mathrm{t}) \in [t, t+T].$$

In a setting in which the derivatives up to $\omega^{(\eta)}$ are included in η, such expression can be recast as

$$x(t+T) = K(T)\eta(t) + J(T)\bar{\omega}(t),$$

where $K(T)$ is as given in (8) and furthermore

$$\bar{\omega}(t) = [\omega^{(r+1)}(t) \quad n(t) \quad \omega^{(r+1)}(\zeta(t))]^T,$$
$$J(T) = \begin{bmatrix} 0 & 0 & J_3(T) \end{bmatrix}, J_3(T) = \frac{T^{(r+2)}}{(\mathrm{r}+2)!}\Gamma_{\omega,(\mathrm{r}+1)}(T)B_\omega.$$

With these considerations, the equations describing the augmented system are

$$\dot{\eta}(t) = \bar{A}\eta(t) + \bar{B}_{\bar{\omega}}\bar{\omega}(t),$$
$$y(t) = \bar{C}\eta(t) + \bar{D}_{\bar{\omega}}\bar{\omega}(t),$$
$$x(t+T) = K(T)\eta(t) + J(T)\bar{\omega}(t),$$

where

$$\bar{B}_{\bar{\omega}} = \begin{bmatrix} 0 & 0 & 0 \\ 0 & 0 & 0 \\ \cdots & \cdots & \cdots \\ I & 0 & 0 \end{bmatrix}, \bar{D}_{\bar{\omega}} = \begin{bmatrix} 0 & H_\omega & 0 \end{bmatrix}.$$

Now, considering the observer

$$\dot{\hat{\eta}} = \bar{A}\hat{\eta} + L(y - \hat{y}), \hat{y} = \bar{C}_\eta\hat{\eta}, \hat{x}(t+T) = K(T)\hat{\eta}(t)$$

and using the KYP lemma as for Method 2, but with a focus on the norm of the transfer matrix norm from the exogenous input $\bar{\omega}$ to the prediction error $e_x(t) = x(t+T) - \hat{x}(t+T)$, one gets the following observer gain design conditions:

$$\begin{bmatrix} \bar{A}^T P + P\bar{A} - Y\bar{C} - \bar{C}^T Y + K^T(T)K(T) & Q \\ Q^T & -\gamma^2 I + J^T(T)J(T) \end{bmatrix} < 0$$

$$Q = P\bar{B}_{\bar{\omega}} - Y\bar{D}_{\bar{\omega}} + K^T(T)J(T), L = P^{-1}Y$$

However, as in the case of Method 2, this approach can be improved by adding weights on the disturbance and the noise, resulting in a structured $H\infty$ synthesis formulation. The extended plant, i.e. the original plant with added weights, to be considered in this case is the one in Fig. 2.

4.4 On the Choice of Weights

In Methods 2 and 3, structured $H\infty$ synthesis is used to accommodate the use of frequency-dependent weights. As in aeronautical instrumentation systems 25 (Hz) is a typical sampling frequency, the weights W_1, W_{1a}, and W_{1b} were chosen as $1/(0.0127s + 1)$. This choice was used for all three predictors, i.e. those for a_x, a_z, and $[\theta, q]$.

For the a_x and a_z predictors, the respective acceleration measurements are available. For the $[\theta, q]$ predictor, the current values of both quantities, θ and q, are available. Concerning noise, a same frequency-dependent weight was used in all channels, supposing for simplicity that the noise figures

are similar. For $W_2(s)$ the high-pass transfer matrix $\kappa s I_p/(s + 30)$, was chosen, with $p = 1$ for the a_x and a_z predictors, and $p = 2$ for the $[\theta, q]$ predictor. $\kappa > 0$ was chosen at design time (see Subsection 5.3).

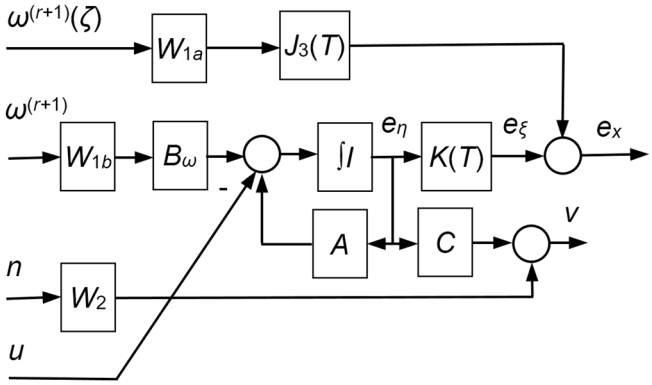

Figure 2 – Generalized plant for gain design with Method 3

5. Implementations for Illustration, Results

5.1 Implementations

The design alternatives described in Section 4 were implemented and verified in Matlab using LMI-related tools, and *hinfstruct* for structured $H\infty$ synthesis.

In a practical implementation of this proposal, observer-predictors for a_x, a_z, and $[\theta, q]$ will be continuously running, such that at all times the updated extended state vectors of these observers are available. At those times in which predictions of u, w, and $\dot{w}$ are demanded to evaluate the aircraft's evolution in the flight envelope plane via predicted V and n_z values, predicted histories for a_x, a_z, and $[\theta, q]$ in the interval $[0, T]$ (T being the prediction horizon) are determined and then used in the integration of the LTV equation (6). Predicted histories for a_x, a_z and $[\theta, q]$ in the interval $[0, T]$ are obtained through the sub-optimal use of the output equations of the respective observers of the form

$$\hat{x}(t+\tau) = \xi(\tau) = K(\tau)\hat{\eta}(t), \tau \in [0, T]\,. \qquad (9)$$

Such calculations are suboptimal, because in Methods 1 and 2, the designer is concerned with $e_\xi(t)$ and in Method 3 with $e_x(t)$, i.e. vector values at one time instant, whereas (9) is used to compute predictions in an interval.

5.2 Scenario for Illustration

The scenario used herein for illustration was defined by using dynamical equation (4), $g = 10$ (m/s^2), initial conditions u_0=500/6 (m/s) (i.e. 300 (km/h)), $w_0 = 0$ (initially leveled flight), $\theta_0 = 5\pi/180$ (rd) (i.e. 5 (°)), $q_0 = 0$, and the following time-histories for a_x, a_z, and m:

$$a_x(t) = 5\sin(\pi t/5) + g\sin(\theta_0), t \in [0, 30\ (\text{s})],$$
$$a_z(t) = -5\sin(\pi t/5) - g\sin(\theta_0), t \in [0, 30\ (\text{s})],$$
$$m(t) = -(2.5\pi/180)(\pi^2/25)\cos(\pi t/5), t \in [0, 30\ (\text{s})].$$

Remarks:

- $a_z(t)$ as above does not "contain" g, and is actually $\Delta a_z(t)$.
- $m(t)$ is such that it takes θ to 0 and back to 5 (°).
- Noises in simulations were generated as 10 (ms) spaced sequences with variances of 10^{-4} (for a_x and a_z) and 10^{-5} (for θ and q). Such choice of variance values was based on arguments in [15].

5.3 Design Parameter Choices and Results

Observer-predictors were used to determine predicted histories for a_x, a_z, and $[\theta, q]$ using the observers discussed in Sections 3 and 4. These predicted histories were fed into the integration of the LTV equation (6) for $[0, T]$-ahead-intervals, $T = 2$ (s) being the prediction horizon. Integration of

(6) was done with Matlab's *ode45*. This resulted in predictions for u, w, and $n_z = \dot{w}/g$ throughout the $[0, T]$-ahead-intervals which, in turn, enabled the prediction of the location in the flight envelope plane throughout the intervals.

Initially, observer-predictors for a_x, a_z, and $[\theta, q]$ were designed and implemented according to Methods 1 to 3. For a_x and a_z prediction a tracking differentiator according to [10] was also implemented for comparison purposes. A bandwidth of $\omega_0 = 10$ (rd/s) was used for that tracking differentiator.

For a_x and a_z predictors according to Methods 1 to 3, $r = 4$ was used. For the $[\theta, q]$ predictors $r = 3$ was used. These choices resulted from design and simulation experiments with $1 \leq r \leq 5$. Smaller r entail less prediction precision; higher r result in larger noise susceptibility.

In Method 1 the following were used: $\alpha = 2$, $\delta = 0.1$ for the a_x and a_z predictors; $\alpha = 1$, $\delta = 0.1$ for the $[\theta, q]$ predictor. In all designs with Method 1, N and M were chosen such that the spectral radius of $(\bar{A} - L\bar{C})$ is less or equal to 80 (see [12] for these and other possible choices).

In Methods 2 and 3, designs were obtained for the extended plants in Figs. 1 and 2, respectively, using structured $H\infty$ synthesis as implemented in Matlab's *hinfstruct*. The weights given in Subsection 4.4 were used with $\kappa = 0.001$ for the a_x and a_z predictors and $\kappa = 0.01$ for the $[\theta, q]$ predictor.

Fig. 3 shows results for the a_z prediction. Results for the a_x prediction are similar and were thus omitted. In this and all further figures, initial observer transients were suppressed. The predictors designed with Methods 2 and 3 show better responses than the tracking differentiator and the predictor designed with Method 1, the main advantage being the smaller noise susceptibility. This is explained by the fact that noise and disturbance were conveniently weighted in the designs with Methods 2 and 3. From the point of view of gain size, Methods 1 to 3 can be considered similar because the norms of the respective gain vectors L were of the same order of magnitude. Thus the results illustrate the added value of the structured $H\infty$ synthesis in this application.

The results for $[\theta, q]$ prediction are shown in Figs. 4 and 5, with basically the same qualitative outcome. The noise susceptibility of the predictor designed with Method 1 is, however, significantly higher in this case.

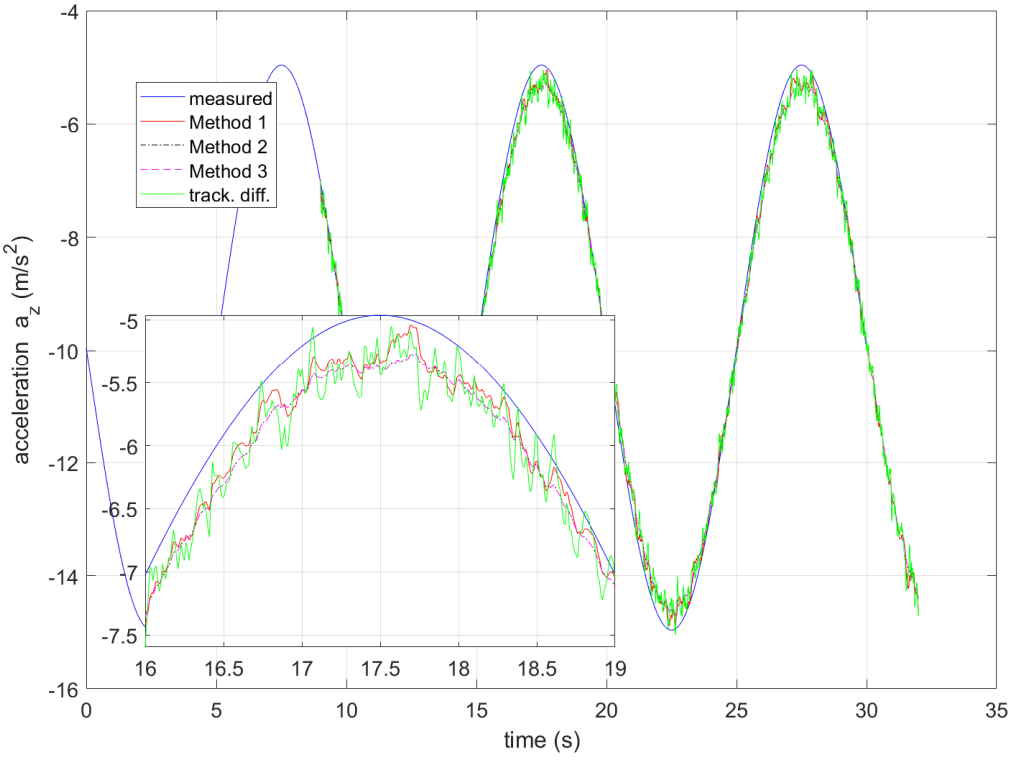

Figure 3 – Real and predicted a_z

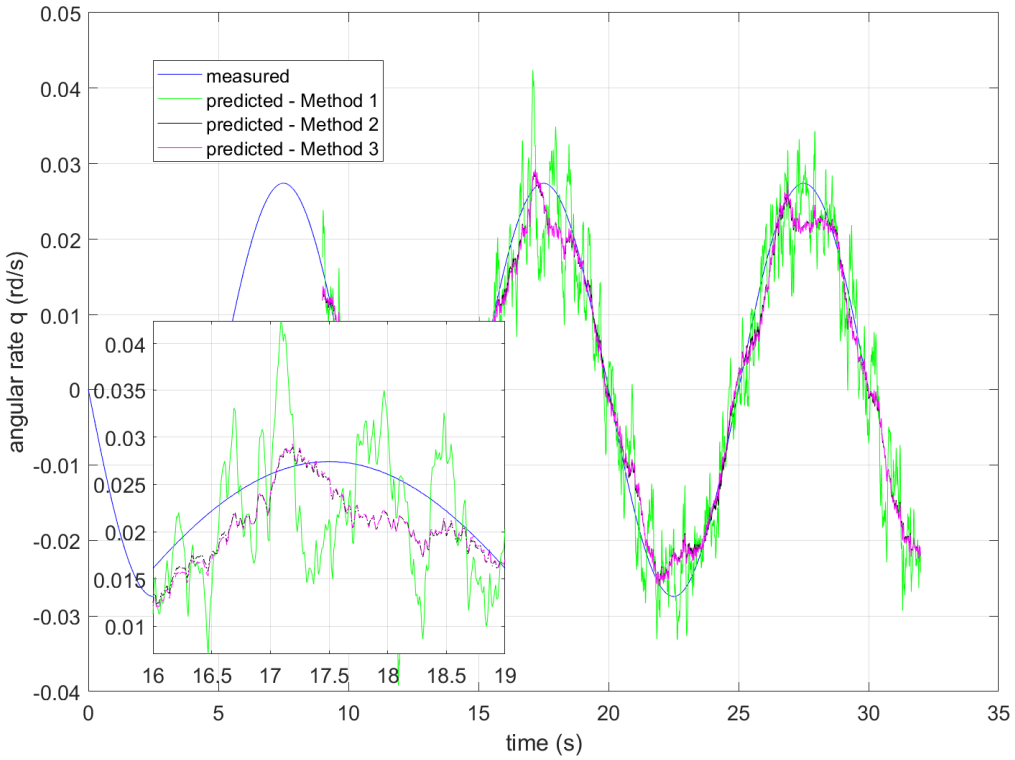

Figure 4 – Real and predicted q

Results of the prediction for flight monitoring in the $V \times n_z$ plane are shown in Figures 6 to 8 for Methods 1 to 3. Mixed realizations were not tested. The red curves show the (real) position evolution of the aircraft in the flight envelope plane. Dotted segments in blue color with [0, T]-ahead predictions are shown, starting with an ○ (at time 0) and ending with an × (at time T).

In Figs. 6 to 8 the smoothing effect of the integration is noticed, especially in the case of Method 1 (Fig. 6). The designs with Methods 2 and 3 show (slightly) better performance in predicting the situation in the flight envelope plane, evidenced by the smaller detachment of the blue dashed segments from the red curve.

6. Conclusions

A rationale and concepts for the predictive flight monitoring of an aircraft within its flight envelope were provided. An illustration of their use in a scenario of longitudinal aircraft motion was presented. The implementation requires the running in parallel of a_x, a_z, and [θ, q] and the integration of a second order LTV differential equation. Three methods for observer-predictor gain design were presented. Furthermore, the performance of a_z predictors was also compared to the performance of the tracking differentiator described in [10].

Several points for additional investigation can be envisioned, e.g. the application to scenarios with longitudinal and lateral motion. Also of interest is a possible quantitative prediction quality assessment. A rationale for this could be as follows. The procedure to predict u, w, and n_z from predicted a_x, a_z, and [θ, q], considered as certain inputs in the integration of equation (6), is equivalent to a prediction through Kalman filter propagation without new values for variables u and w. The propagation of the associated covariance in a Kalman filter, not needed for predicted value calculation in such circumstances, would, however, be valuable in assessing the prediction's reliability. Thus such propagation shall be the object of future research. It includes the quest for covariance information of the driving signals in (6), i.e. the a_x, a_z, and [θ, q] predictions, as well as how to cope with the fact that the state matrix in (6) is "de facto" a matrix affected by the uncertainty in the predicted q history.

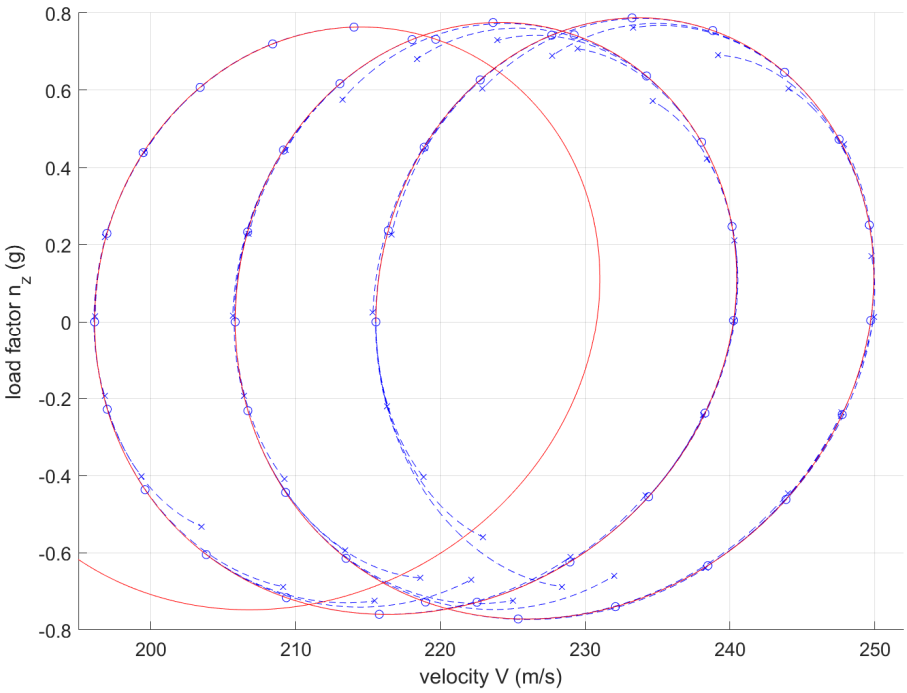

Figure 6 - Prediction in the $V \times n_z$ plane with Method 1: real evolution red; $[0,\ T]$-ahead predictions dotted blue ○—x

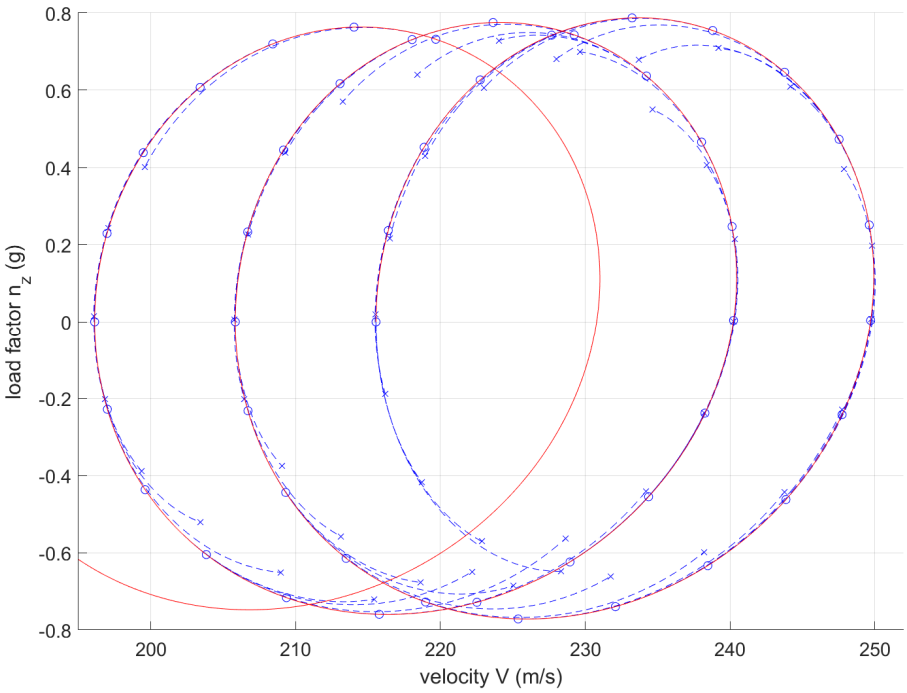

Figure 7- Prediction in the $V \times n_z$ plane with Method 2: real evolution red; $[0,\ T]$-ahead predictions dotted blue ○—x

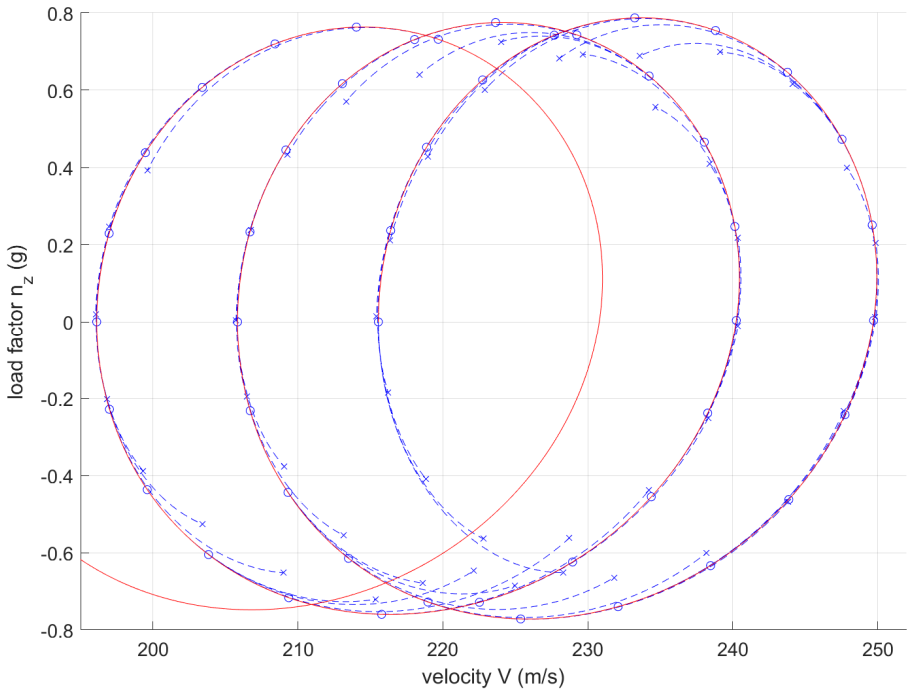

Figure 8 - Prediction in the $V \times n_z$ plane with Method 3: real evolution red; [0, T]-ahead predictions dotted blue ○--x

7. Contact Author Email Address

For more information, contact the first author at kienitz@ieee.org.

8. Copyright Statement

The authors confirm that they, and/or their company or organization, hold copyright on all of the original material included in this paper. The authors also confirm that they have obtained permission, from the copyright holder of any third party material included in this paper, to publish it as part of their paper. The authors confirm that they give permission, or have obtained permission from the copyright holder of this paper, for the publication and distribution of this paper as part of the ICAS proceedings or as individual off-prints from the proceedings.

9. Acknowledgments

The first author acknowledges partial support through grants from: (a) Grupo Tordesillas / Fundación Carolina, Spain; and (b) CNPq, Brazil (grant #304557/2021-8).

References

[1] N. Glīzde, “Plotting the flight envelope of an unmanned aircraft system air vehicle,” *Transport and Aerospace Engineering*, vol. 4, no. 1, pp. 80–87, 2017, doi: 10.1515/tae-2017-0010.

[2] K. Well, “Aircraft control laws for envelope protection,” in *AIAA GNC Conference & Exhibit*, Reston, VA, 2006, p.6055.

[3] H. Ye, M. Chen, Q. Wu, “Flight envelope protection control based on reference governor method in high angle of attack maneuver,” *Mathematical Problems in Engineering*, p. 254975, 2015, doi: 10.1155/2015/254975.

[4] S. Sun and C.C. de Visser, “Quadrotor safe flight envelope prediction in the high-speed regime: a Monte-Carlo approach,” in *AIAA Scitech 2019 Forum*, San Diego, CA, 2019, p. 0948.

[5] Z. Lu *et al.*, “Flight envelope prediction via optimal control-based reachability analysis,” *Journal of Guidance, Control, and Dynamics*, vol. 45, no. 1, pp. 185-195, 2022, doi: 10.2514/1.G006219.

[6] Z. Lu *et al.*, “Maneuverability set estimation and trajectory feasibility evaluation for eVTOL aircraft,” *Journal of Guidance, Control, and Dynamics*, vol. 46, no. 6, pp. 1184-1196, 2023, doi: 10.2514/1.G007109.

[7] A. Castillo and P. Garcia, “Predicting the future state of disturbed LTI systems: A solution based on high-order observers,” *Automatica*, v. 124, p. 109365, 2021, doi: 10.1016/j.automatica.2020.109365.

[8] R.C. Nelson, *Flight stability and automatic control*. 2nd edition, New York: McGraw Hill, 1998.

[9] C.B. de Mendonça, E. M. Hemerly, and L.C.S. Góes, “Adaptive stochastic filtering for online aircraft flight path reconstruction,” *Journal of Aircraft*, vol. 44, no. 5, pp. 1546-1558, 2007, doi: 10.2514/1.27625.

[10] R. Sanz, P. García, and P. Albertos, “Enhanced disturbance rejection for a predictor-based control of LTI systems with input delay,” *Automatica*, vol. 72, 205-208, 2016, doi: 10.1016/j.automatica.2016.05.019.

[11] V. Léchappé, E. Moulay, F. Plestan, A. Glumineau, and A. Chriette, “New predictive scheme for the control of LTI systems with input delay and unknown disturbances,” *Automatica*, vol. 52, pp. 179-184, 2015, doi: 10.1016/j.automatica.2014.11.003.

[12] M. Chilali, P. Gahinet, and P. Apkarian, “Robust pole placement in LMI regions,” *IEEE Transactions on Automatic Control*, vol. 44, no. 12, pp. 2257-2270, 1999, doi: 10.1109/9.811208.

[13] P. Apkarian, D. Noll, (2006). “Nonsmooth H-infinity synthesis,” *IEEE Transactions on Automatic Control*, vol. 51, no. 1, pp. 71-86, 2006, doi: 10.1109/TAC.2005.860290.

[14] S. Skogestad and I. Postlethwaite, *Multivariable feedback control: analysis and design*. 2nd edition, Chichester: John Wiley & Sons, 2005.

[15] C.B. de Mendonça, “Análise de compatibilidade de dados de ensaio em voo e calibração dos dados do ar em tempo real com filtragem estocástica adaptativa,” Doctoral Thesis, Instituto Tecnológico de Aeronáutica, São José dos Campos, SP, Brazil, 2005.